Astronomy
&
Astrophysics

Upper limit for the D_2H^+ ortho-to-para ratio in the prestellar core 16293E (CHESS)[*],[**]

C. Vastel[1,2], P. Caselli[3], C. Ceccarelli[4], A. Bacmann[4], D. C. Lis[5], E. Caux[1,2], C. Codella[6],
J. A. Beckwith[7], and T. Ridley[3]

[1] Université de Toulouse, UPS-OMP, IRAP, Toulouse, France
e-mail: charlotte.vastel@irap.omp.eu
[2] CNRS, Institut pour la Recherche en Astrophysique et Planétologie, 9 Av. Colonel Roche, BP 44346,
31028 Toulouse Cedex 4, France
[3] School of Physics and Astronomy, University of Leeds, Leeds LS2 9JT, UK
[4] Université Joseph Fourier and CNRS, Institut de Planétologie et d'Astrophysique, Grenoble, France
[5] California Institute of Technology, Cahill Center for Astronomy and Astrophysics, Pasadena, CA 91125, USA
[6] INAF Osservatorio Astrofisico di Arcetri, Largo E. Fermi 5, 50125 Firenze, Italy
[7] School of Earth and Environment, University of Leeds, Leeds LS2 9JT, UK

ABSTRACT

The H_3^+ ion plays a key role in the chemistry of dense interstellar gas clouds where stars and planets are forming. The low temperatures and high extinctions of such clouds make direct observations of H_3^+ impossible, but lead to large abundances of H_2D^+ and D_2H^+, which are very useful probes of the early stages of star and planet formation. The ground-state rotational ortho-D_2H^+ $1_{1,1}$–$0_{0,0}$ transition at 1476.6 GHz in the prestellar core 16293E has been searched for with the *Herschel* HIFI instrument, within the CHESS (Chemical HErschel Surveys of Star forming regions) Key Program. The line has not been detected at the 21 mK km s^{-1} level (3σ integrated line intensity). We used the ortho-H_2D^+ $1_{1,0}$–$1_{1,1}$ transition and para-D_2H^+ $1_{1,0}$–$1_{0,1}$ transition detected in this source to determine an upper limit on the ortho-to-para D_2H^+ ratio as well as the para-D_2H^+/ortho-H_2D^+ ratio from a non-local thermodynamic equilibrium analysis. The comparison between our chemical modeling and the observations suggests that the CO depletion must be high (larger than 100), with a density between 5×10^5 and 10^6 cm^{-3}. Also the upper limit on the ortho-D_2H^+ line is consistent with a low gas temperature ($\sim$11 K) with a ortho-to-para ratio of 6 to 9, i.e. 2 to 3 times higher than the value estimated from the chemical modeling, making it impossible to detect this high frequency transition with the present state of the art receivers.

Key words. astrochemistry – ISM: individual objects: 16293E – ISM: abundances – line: identification – radiative transfer

1. Introduction

In the recent years, the chemistry of dark clouds and star forming regions has constantly been revised with the discovery of multiply deuterated molecules: D_2CO (Turner 1990; Ceccarelli et al. 1998), ND_2H (Roueff et al. 2000), D_2S (Vastel et al. 2003), ND_3 (Lis et al. 2002; van der Tak et al. 2002), CHD_2OH, CD_3OH (Parise et al. 2002, 2004) and D_2H^+ (Vastel et al. 2004). Two main pathways can be invoked for understanding the observed large deuterium fractionation. The first is based on grain chemistry (Tielens 1983). Vastel et al. (2003) and Parise et al. (2004) showed that grain chemistry models require a very high atomic D/H ratio accreting on the grains in order to explain their high deuterium fractionation ratio that could not be reproduced by gas-phase modeling at that time. New models can now reproduce the observed abundance of the multi-deuterated isotopologues of formaldehyde and methanol, both formed in the last stage of the prestellar phase (Taquet et al. 2012). The second pathway for forming deuterated molecules is based on

gas-phase chemistry and results from the ion-molecule deuterium exchange reactions taking place at low temperatures. In this scenario, deuterated molecules are produced through successive reactions starting with H_2D^+, dominant at temperatures lower than 20 K, CH_2D^+ or C_2HD^+, dominant at higher temperatures (Roberts & Millar 2000; Gerlich et al. 2002). H_2D^+ has proven to be a very good probe of the dense cold cores, where CO disappears from the gas phase and is depleted onto the dust grains (Caselli et al. 2003, 2008).

Phillips & Vastel (2003) pointed out that the deuteration should be extended beyond H_2D^+, to D_2H^+ and D_3^+ and suggested that the detection of the D_2H^+ ion might be possible. Calculations including all possible deuterated isotopomers of H_3^+ have confirmed that, in dense CO depleted regions, the abundance of D_2H^+ will be similar to that of H_2D^+, and the D/H ratio will be largely enhanced (Roberts et al. 2003, 2004; Walmsley et al. 2004; Ceccarelli & Dominik 2005).

D_2H^+ in its para form was detected for the first time in the prestellar core 16293E by Vastel et al. (2004), showing its importance, as well as that of D_3^+, in determining the total deuterium abundance in the gas phase. This dense core, revealed by amonia emission (Mizuno et al. 1990), is sheltered in the dense cloud L1689N (see Wootten & Loren 1987), in the Ophiuchi region (distance 120 pc: Loinard et al. 2008) and has been revealed by
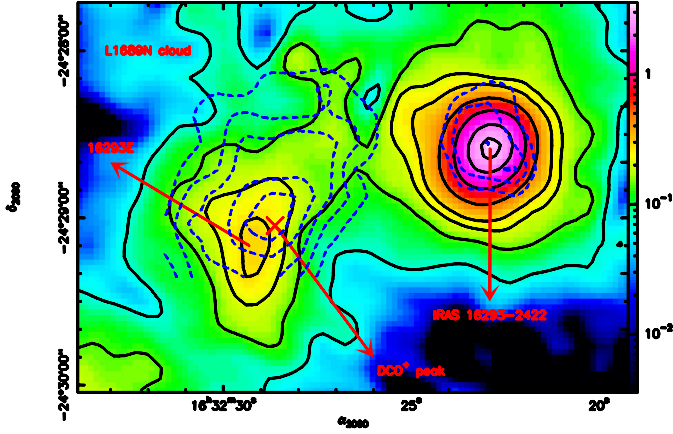
Fig. 1. Continuum map at 1.3 mm convolved to 15″ with black contours at 4%, 6%, 8%, 15%, 30%, 60%, and 90% of the peak located at the IRAS 16293-2422 position (6.7 Jy in a 1500 beam). Dashed blue lines show the distribution of the DCO⁺ 3–2 integrated intensity between 2.8 and 5 km s⁻¹, with contour levels contour levels are 50%, 60%, 70%, 80% and 90% of the peak (integrated over velocities between 2.8 and 5 km s⁻¹). The cross represent the position towards which H_2D^+ and D_2H^+ have been observed.

Fig. 2. Para-D_2H^+ ($1_{1,0}-1_{0,1}$) and ortho-D_2H^+ ($1_{1,0}-1_{0,1}$) transitions observed with the CSO and *Herschel*/HIFI. The Wide Band Spectrometer is represented in red, and the High Resolution Spectrometer in black.

millimeter lines and continuum emission. This cloud, also harboring a young binary protostellar object (IRAS 16293-2422 A and B) and bipolar outflows (named Rho Oph East by Fukui et al. 1986), has been extensively observed, revealing an extreme molecular deuteration in particular towards the cold dense core, named 16293E by Loinard et al. (2001) and Castets et al. (2001). Note that this core has been called ρ Oph E (as in Rho Oph East referring to the outflow emanating from IRAS 16293-2422) by Saito et al. (2000) and Gérin et al. (2001). However, we decided to use the name 16293E since ρ Oph E already refers to another condensation within the L1688 cloud in the Ophiuchi complex (Loren et al. 1990) and, therefore, is confusing. We present here recent *Herschel*/HIFI observations obtained within the *Herschel* guaranteed time Key Program CHESS, and modeling of both ground state transitions of para- and ortho-D_2H^+, as well as ortho-H_2D^+, using the recent collisional coefficients with ortho- and para-H_2 (Hugo et al. 2009).

Figure 1 shows the 1.3 mm continuum map as well as the DCO⁺ contour map (blue) (Lis et al. 2002). Studies of the gas kinematics using CO, HCN, $H^{13}CO^+$, HCO⁺ and DCO⁺ tracers lead to the conclusion that the deuterium peak is a part of the ambient cloud that is pushed and compressed by the outflow (Lis et al. 2002). Indeed this shock could have released deuterated species, that were condensed on the dust grains, into the gas phase with a subsequent cooling of the gas to lower temperatures. This effect, combined with the low temperature gas-phase chemistry in the high-density shock-compressed gas leads to a high molecular deuteration as observed in: DNC (9%: Hirota et al. 2001), D_2CO (40% ± 20% Loinard et al. 2001; Ceccarelli et al. 2002), N_2D^+ (Gérin et al. 2001), NH_2D (19% Mizuno et al. 1990; Loinard et al. 2001; Roueff et al. 2005), ND_2H (4%: Mizuno et al. 1990; Loinard et al. 2001; Lis et al. 2006), DCO⁺ and DCN (∼10%: Lis et al. 2002), HDS (Vastel et al. 2003), D_2H^+ (Vastel et al. 2004), HDO (Stark et al. 2004), ND_3 (0.1%: Roueff et al. 2005). Because no far-infrared or submillimeter point source has been found, the source can be classified as a prestellar core, the early phase of the formation of a protostellar object, before gravitational contraction occurs.
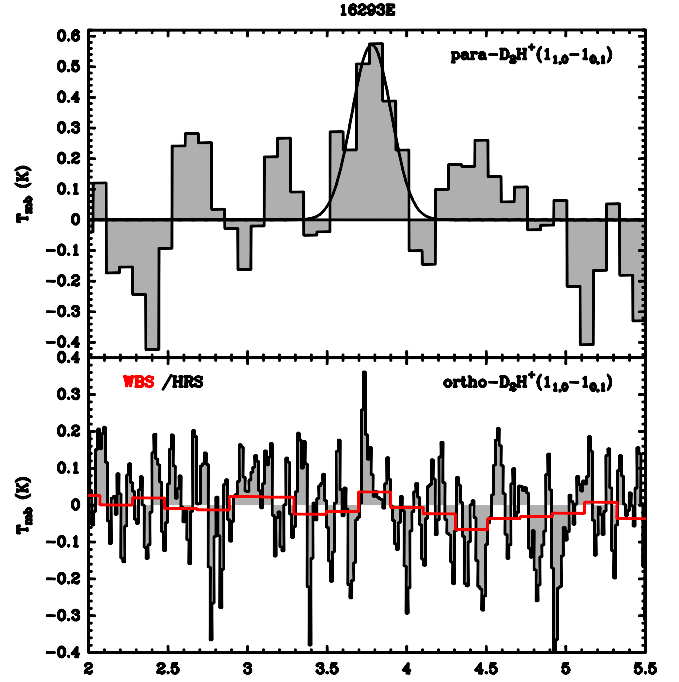
2. Observations and data reduction

The para-D_2H^+ ground state transition was observed towards the prestellar core 16293E with the HIFI instrument (de Graauw et al. 2010) on board the *Herschel* Space Observatory (Pilbratt et al. 2010), as part of the *Herschel* guaranteed time Key Program CHESS (Ceccarelli et al. 2010).

A pointing at a frequency centered on the D_2H^+ line (∼1476.6 GHz) with the band 6a HEB receiver was performed on February 16, 2011 using the pointed Double Beam Switch (DBS) mode with optimization of the continuum. In this mode, both the HIFI Wide Band Spectrometer (WBS) – providing a spectral resolution of 1.1 MHz (∼0.2 km s⁻¹) over an instantaneous bandwidth of 2.4 GHz – and the HIFI High Resolution Spectrometer (HRS) – providing a spectral resolution of 125 kHz over an instantaneous bandwidth of 0.12 GHz – were used. The DBS reference positions were situated approximately 3′ East and West of the source. The HIFI beam size at the observed frequency is about 14″, and the main beam and forward efficiencies are about 0.72 and 0.96, respectively (Roelfsema et al. 2012). The data have been processed using the standard HIFI pipeline up to level 2 with the ESA-supported package HIPE 8.0 (Ott 2010). The on-source integration time for this observation was 18 157 s. FITS files from level 2 data were created and translated into CLASS/GILDAS format for subsequent data reduction and analysis. For each scan, a low order polynomial baseline was fitted outside the line window. The antenna temperatures were finally converted to the T_{mb} scale, using the theoretical values of the main beam and forward efficiencies given above. We present in Fig. 2 this observation as well as the para ground state transition observed at the Caltech Submillimeter Observatory (CSO) (Vastel et al. 2004). Both observations were pointed towards the DCO⁺ peak emission, at coordinates $\alpha_{2000} = 16^h32^m28\overset{s}{.}62$, $\delta_{2000} = -24°29'2.7''$ (see for example Roueff et al. 2005, Fig. 9). Note that the coordinates

Table 1. Derived parameters of the ortho-H$_2$D$^+$ transitions as well as the ortho and para D$_2$H$^+$ fundamental lines. DCO$^+$ 3–2 and 5–4 transitions used in Lis et al. (2002) are also quoted using the estimated frequencies from Caselli & Dore (2005).

Species	Transition	Frequency GHz	Telescope	Beamsize (″)	$\int T_{mb}\, dV$ (mK km s^{-1})	rms mK	Binsize (km s^{-1})	ΔV (km s^{-1})	V_{LSR} (km s^{-1})
ortho-H$_2$D$^+$	$1_{1,0}$–$1_{1,1}$	372.421385	CSO	20	720	80	0.080	0.36 ± 0.04	3.59 ± 0.02
para-D$_2$H$^+$	$1_{1,0}$–$1_{0,1}$	691.660483	CSO	11	183	170	0.080	0.29 ± 0.05	3.78 ± 0.02
ortho-D$_2$H$^+$	$1_{1,1}$–$0_{0,0}$	1476.605708	HIFI/HRS	14	≤30	120	0.012		
ortho-D$_2$H$^+$	$1_{1,1}$–$0_{0,0}$	1476.605708	HIFI/WBS	14	≤21	21	0.203		
DCO$^+$	3–2	216.1125822	CSO	35	3235	94	0.134	0.67 ± 0.03	3.55 ± 0.01
DCO$^+$	5–4	360.1697783	CSO	20	528	109	0.081	0.54 ± 0.03	3.65 ± 0.01

Notes. A discussion on the V_{LSR} can be found at the end of Sect. 2.

in Vastel et al. (2004) were not correctly quoted in the text and should be replaced by the here quoted coordinates.

The two nuclear-spin species of H$_2$D$^+$ and D$_2$H$^+$ (ortho and para) are considered separately. The parameters of the ortho- and para-D$_2$H$^+$ and ortho-H$_2$D$^+$ ground transitions are obtained using the CASSIS[1] software, which takes into account the ortho and para forms separately, with an independent computation of the partition function (cf. Formalism for the CASSIS software, http://cassis.irap.omp.eu/), and are reported in Table 1. The Einstein coefficient for the ortho-D$_2$H$^+$ transition ($\sim 3 \times 10^{-3}$ s^{-1}) is much larger than for the para-D$_2$H$^+$ ($\sim 4.6 \times 10^{-4}$ s^{-1}) and ortho-H$_2$D$^+$ ($\sim 1.1 \times 10^{-4}$ s^{-1}) transition, since it varies as a function of ν^3. Note that we adopt here the most recent measurement of Amano & Hirao (2005) of the para-D$_2$H$^+$ line frequency (691.660483 GHz), 372.421385 GHz for the ortho-H$_2$D$^+$ transition and 1476.605708 GHz for the ortho-D$_2$H$^+$ transition (Asvany et al. 2008). From a simple Gaussian fitting function, the resulting V_{lsr} are (3.78 ± 0.02) km s^{-1} for the para-D$_2$H$^+$ transition and (3.59 ± 0.02) km s^{-1} for the ortho-H$_2$D$^+$ transition (statistical uncertainty from the fit). The minimum difference between the lines is 0.15 km s^{-1}, compatible with the $\sim$0.1 km s^{-1} resolution of the acousto-optic spectrometer at 692 GHz, and 0.04 km s^{-1} at 372 GHz. A difference in the observed V_{lsr} is found (exploitation of the data mentioned in Lis et al. 2002, but not published) in the DCO$^+$ 5–4 (3.65 ± 0.01 km s^{-1}) and 3–2 (3.55 ± 0.01 km s^{-1}) transitions. The quoted uncertainties correspond to the Gaussian fit and the line parameters are listed in Table 1. A larger difference in the line center velocity is noticeable comparing the ortho-ND$_2$H $1_{1,1}$–$0_{0,0}$ (V_{lsr} = 3.64 km s^{-1}) and $1_{1,1}$–$0_{0,0}$ (V_{lsr} = 3.60 km s^{-1}) transitions (Lis et al. 2006), as well as the ortho-NH$_2$D $1_{1,1}$–$1_{0,1}$ (V_{lsr} = 3.65 km s^{-1}) and para-NH$_2$D $1_{1,1}$–$1_{0,1}$ (V_{lsr} = 3.67 km s^{-1}) transitions (Loinard et al. 2001), with the ND$_3$ 1_0–0_0 (V_{lsr} = 3.35 km s^{-1}) transition (Roueff et al. 2005). Such a difference could be explained by dynamical motions in this source that cannot be reproduced with a simple Gaussian fitting function. The interaction between the outflow of IRAS 16293-2422 and the cold core 16293E is likely to produce a velocity shift compared to the L1689N parental cloud, with a difference between the non deuterated species and their increasingly deuterated forms. The difference in the beam sizes of the numerous observations may be responsible for such a variation as well. The single-dish observations do not allow to conclude.

The 3σ upper limit on the integrated line intensity, using the Wide Band Spectrometer, has been derived following the relation:

$$3\sigma \text{ (K km s}^{-1}) = 3 \times \text{rms} \times \sqrt{2 \times dv \times FWHM} \qquad (1)$$
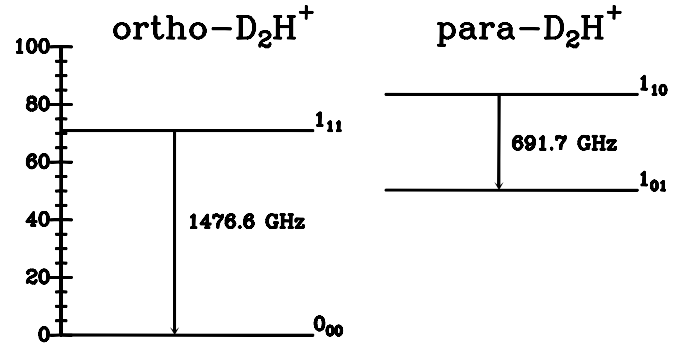
Fig. 3. Diagram of the lowest energy levels (in Kelvins) of the D$_2$H$^+$ molecule.

with rms (root mean square) in K, dv, the channel width, in km s^{-1} and $FWHM$ (Full Width at Half Maximum) in km s^{-1}. We assumed $FWHM$ = 0.29 km s^{-1}, which is the para-D$_2$H$^+$ emission line width.

3. Discussion

3.1. Line widths

The line widths are listed in Table 1. The expected thermal line width varies with the kinetic temperature (T) as:

$$\Delta v_T (\text{km s}^{-1}) = 2\sqrt{2\ln 2} \times \sqrt{\frac{kT}{m}}, \qquad (2)$$

where k is the Boltzman constant and m is the molecular weight. The ortho-H$_2$D$^+$ line width corresponds to a 11.3 K gas, comparable with the 9.2 K temperature found for para-D$_2$H$^+$. However, the uncertainty in the fit of the line, using the Levenberg-Marquardt method, should be taken into account leading a temperature of 11.3 ± 1.8 K for H$_2$D$^+$ and 9.2 ± 3.2 K for D$_2$H$^+$. The resulting range for the kinetic temperature is therefore [9.5–12.4] K taking into account both ions.

The observed (o-p) ND$_2$H line width (about 0.45 km s^{-1} for the $1_{1,1}$–$0_{0,0}$ transitions; Lis et al. 2006), ND$_3$ (0.44 km s^{-1}; Roueff et al. 2005) as well as the DCO$^+$ line width (about 0.5 km s^{-1} for the 5–4 transition, less optically thick than the 3–2 transition; Lis et al. 2002) and the N$_2$D$^+$ line width (0.32 km s^{-1} for the 3–2 transition; Gérin et al. 2001) are systematically larger than the thermal line widths of 0.16, 0.12 and 0.16 km s^{-1} respectively for a 10 K kinetic temperature. Considering the high critical densities for the (o-p) ND$_2$H and ND$_3$ transitions (larger than 10^6 cm^{-3}), it seems that systematic motions occur even in the dense part of the cloud. Also, at large enough densities/depletions, one expect to have the light ions left

as the main tracers of the gas. This further confirms that H_2D^+ and D_2H^+ remain the only tracers of the cold, dense and CO/N_2 depleted central region where other molecular tracers are largely condensed onto the dust grains, rather than the lower density envelope when turbulence takes over.

3.2. H_2D^+ and D_2H^+ non-LTE modeling

The H_2 density is a critical parameter for the interpretation of our deuterated ions observations. CO observations of the 3–2, 4–3, 6–5 transitions give a lower limit for the molecular hydrogen density of 5×10^3 cm^{-3} (Lis et al. 2002). In their analysis, Lis et al. (2002) used a kinetic temperature of 12 K (based on NH_3 observations of Menten et al. 1987) and a density of 5×10^5 cm^{-3}, consistent with their observed DCO^+ (5–4)/(3–2) and N_2D^+ (4–3)/(3–2) line ratios. From 450 and 850 μm continuum maps Stark et al. (2004) inferred an isothermal dust temperature $T = 16$ K and peak density of 1.6×10^6 cm^{-3}. Note however that their dust peak emission does not correspond to the peak of deuterated molecules (about 15″ away) that we are studying in the present paper. This could be due to the release of the deuterated species that were condensed on the dust grains by the interaction between the outflow from IRAS 16293-2422 and the cold core 16293E. This compression is then likely to cool the gas to lower temperatures. These observations possibly trace the parental cloud of the prestellar core 16293E. We will therefore consider in the following study densities between 10^5 and 10^6 cm^{-3} and kinetic temperatures between 9 and 16 K (see Sect. 3.1).

From the recent computations of the collision rates (Hugo et al. 2009), the critical densities for the ortho-H_2D^+, ortho-D_2H^+ and para-D_2H^+ transitions are $\sim 1.3 \times 10^5$ cm^{-3}, $\sim 7 \times 10^6$ cm^{-3} and $\sim 5.6 \times 10^5$ cm^{-3} respectively, using the Einstein coefficients from Ramanlal & Tennyson (2004), 1.2×10^{-4}, 3.3×10^{-3} and 5.1×10^{-4} s^{-1} respectively. From the large difference between the critical densities, the ortho-D_2H^+ transition will trace denser regions than the para transition. Since the typical density in the core seems to be less than these critical densities, a local thermodynamic equilibrium (LTE) approximation is not applicable. In Vastel et al. (2004), only LTE modeling could be performed because the collision rates were not available at that time. We produced collisional files, assuming a simple 2 level system, using the inelastic state-to-state rate coefficients for the ortho and para ground transitions of H_2D^+ and D_2H^+ in collision with para and ortho H_2, as a function of temperature. We used the non-LTE radiative transfer code RADEX (van der Tak et al. 2007) in the large velocity gradient (LVG) approximation with the collisional files that were created for these species. We could consider in the following non-LTE modeling two values for the H_2 ortho-to-para ratio of 3 (highest value at thermodynamic equilibrium) and 0 (only collisions with para H_2). However, the similarities of the collision coefficients with ortho and para H_2 for (o, p)H_2D^+ or (o, p)D_2H^+ will lead to a very small difference in the derived column densities.

The variation of the para-D_2H^+ to ortho-H_2D^+ ratio as a function of the gas temperature, for densities of 1×10^5 (green), 5×10^5 (blue) and 1×10^6 (red) cm^{-3}, are presented in Fig. 4 (thick lines) and the upper limit on the ortho-to-para D_2H^+ ratio is presented in Fig. 5 (thick lines). Note that a selection on the optical depth has been performed ($\tau < 100$), since the excitation temperature found using RADEX may then not be representative of the emitting region. The optical depth for the ortho-D_2H^+ transition is lower than 100 for kinetic temperatures larger than ~ 10.5 K.

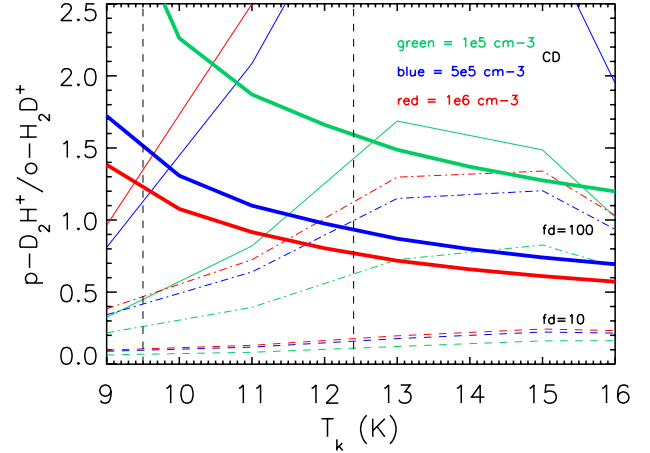**Fig. 4.** Variation of the para–D_2H^+ to ortho–H_2D^+ ratio as a function of the gas temperature, for densities of 1×10^5 (green), 5×10^5 (blue) and 1×10^6 (red) cm^{-3}. The thick lines show the ratio derived from observations, using non-LTE modeling, whereas the thin lines show the chemical model results. Three depletion factors at steady-state are presented: complete depletion (CD: solid lines), depletion factor =100 (dot-dashed lines) and depletion factor =10 (dashed lines). The thin dashed vertical lines present the [9.5–12.4] K range.

3.3. Full chemical modeling

The chemical network used here has been collected from various sources. First, a reduced chemical network based on the Nahoon code was obtained from the KIDA[2] database (Wakelam et al. 2012). The network contains species with three or less elements and includes hydrogen, helium, carbon, nitrogen and oxygen. The reduced Nahoon code has then been modified to include deuterium and deuterated species, with H_2, HD and D_2 forming on grain surfaces. Finally, the spin states of all isotopologues of H_2 and H_3^+ were included. The rate coefficients of the new reactions were taken from Sipilä et al. (2010), Hugo et al. (2009), Flower et al. (2004) and Walmsley et al. (2004), choosing the most recent values in case of multiple choice. The reaction balancing routine within the Nahoon program (the one which checks the reaction list, to make sure that reactants and products have the same number of elements and charges) had to be modified after the inclusion of the different spin states, to avoid to balance spin states between reactants and products (as spin states are not conserved). For this purpose, different spin states were labelled adding an extra column in the element and species definition file. In this column we assigned –1 to the lower spin state and +1 to the higher spin state of all isotopologues of H_2 and H_3^+ (para-D_3^+ has been assigned a value of +2 as it is the highest of three spin states). All other species have a zero in the corresponding column, indicating that no spin state is considered. The H_2 self shielding data has not been modified but new parameters for the self shielding of HD and D_2 have been introduced and have been each set to initially be equal to that of H_2. Coulomb focusing was taken into account for reactions involving negatively charged ions on neutral grains (Draine & Sutin 1987). Only neutral and negatively charged grains are present in the network. The final chemical network includes over 3500 reactions involving nearly 130 different species. The full chemical network used in this work is available at the CDS. Comparison with previous work and a parameter space exploration will be presented by Kong et al. (in prep.).
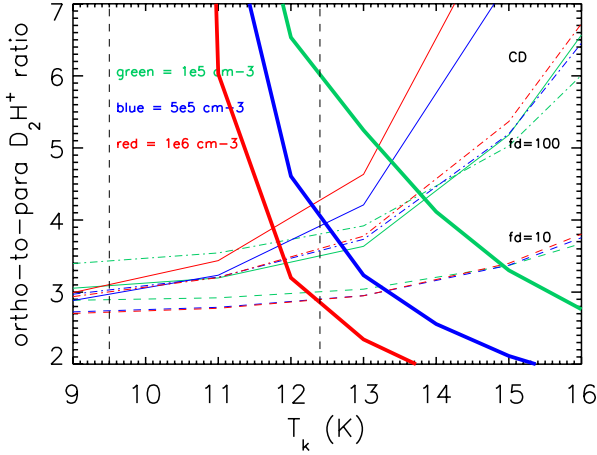
---

[2] http://kida.obs.u-bordeaux1.fr/models

Fig. 5. Variation of the ortho-to-para D$_2$H$^+$ ratio as a function of the gas temperature, for densities of 1×10^5 (green), 5×10^5 (blue) and 1×10^6 (red) cm^{-3}. The thick lines show the ratio derived from observations, using non-LTE modeling, and can be considered as upper limits, whereas the thin lines show the chemical model results. Three depletion factors at steady-state are presented: complete depletion (CD: solid lines), depletion factor =100 (dot-dashed lines) and depletion factor =10 (dashed lines). The thin dashed vertical lines present the [9.5–12.4] K range.

Fig. 6. Prediction of the ortho-to-para H$_2$D$^+$ ratio as a function of the gas temperature, for densities of 1×10^5 (green), 5×10^5 (blue) and 1×10^6 (red) cm^{-3}. Three depletion factors at steady-state are presented: complete depletion (CD: solid lines), depletion factor =100 (dot-dashed lines) and depletion factor =10 (dashed lines). The thin dashed vertical lines present the [9.5–12.4] K range.

A range of H$_2$ volume densities (1×10^5, 5×10^5, 1×10^6 cm^{-3}), kinetic temperatures (9, 11, 13, 15, and 16 K), and depletion factors ($\equiv$undepleted abundance / depleted abundance =10, 100, infinity) of all the elements heavier than helium (C, N and O) have been explored and followed in time until the system reaches equilibrium. Since the CO molecule is the main destroyer of the H$_3^+$ ion (and its deuterated counterparts), we simulate three depletion values at steady-state: complete depletion, and elemental depletion factor of 10 and 100 corresponding to CO depletion factors of about 14 and 140, respectively, at equilibrium. From Lis et al. (2002), C^{18}O observations at the deuterium peak of 16293E lead to a CO depletion factor (average along the line of sight) of ~10, representing a lower limit for the central core traced by D$_2$H$^+$. Considering the overall parameters in the chemical modeling we adopt the conservative values of 3×10^{-17} s^{-1} for the cosmic ionization rate, 0.01 for the dust to gas ratio, and 0.1 μm for the grain radius.

Figures 4–6 show the predictions (thin lines) of the model at equilibrium (reached in 2×10^5 years for the complete depletion case, 5×10^5 years for a depletion factor of 100 and 2×10^6 years for a depletion factor of 10) for temperatures between 9 and 16 K for three densities. The para-D$_2$H$^+$/ortho-H$_2$D$^+$ ratio increases with the depletion factor: indeed the disappearance of the CO molecule from the gas phase leads to the reactions of HD with H$_3^+$ with an increasing production of its deuterated counterparts (Phillips & Vastel 2003). Also the increase of the ortho-to-para D$_2$H$^+$ ratio with the depletion factor can be explained by the fact that the reactions with HD, ortho-D$_2$ and para-D$_2$ converting para-D$_2$H$^+$ into ortho-D$_2$H$^+$ are dominant compared to the reverse reactions (Hugo et al. 2009). From Eqs. (4) and (5) we can say that a low ortho-H$_2$ value leads to a very high D$_3^+$ abundance for densities larger than 10^5 cm^{-3}. Indeed the D$_3^+$ ion is likely to be the dominant ion in such high-density regions: e.g. Fig. 3 from Flower et al. (2006) and Fig. 2 from Sipilä et al. (2010). The ortho-to-para D$_2$H$^+$ ratio consequently increases as the depletion factor increases, as seen in Fig. 5. The ortho-to-para H$_2$ ratio should be taken into account in the overall chemistry, since it is critical for the degree of deuteration
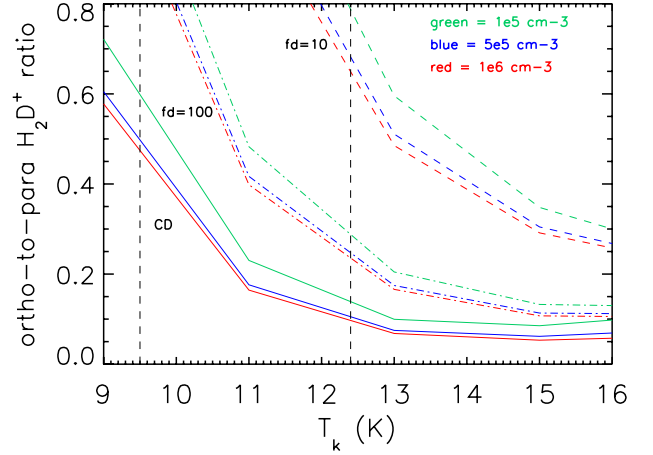

Fig. 7. Variation of the ortho-to-para H$_2$ ratio as a function of the kinetic temperature, for densities of 1×10^5 (green), 5×10^5 (blue) and 1×10^6 (red) cm^{-3}. Three depletion factors at steady-state are presented: complete depletion (CD: solid lines), depletion factor =100 (dot-dashed lines) and depletion factor =10 (dashed lines). The thin dashed vertical lines present the [9.5–12.4] K range.
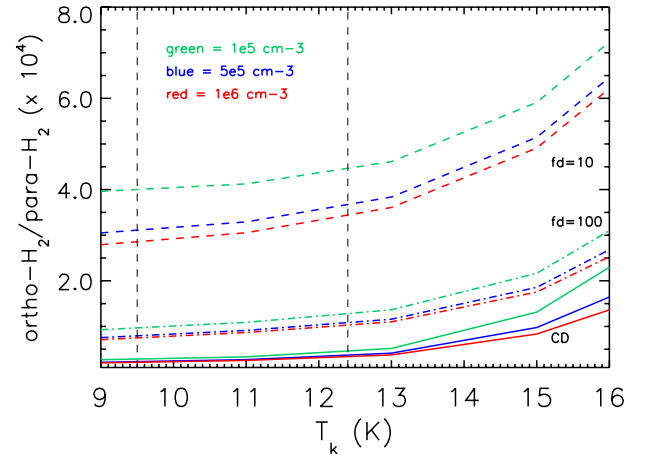
of H$_3^+$. Increasing the depletion factor leads to a local decrease of the CO abundance. Therefore H$^+$ and H$_3^+$ will mainly react with ortho-H$_2$ (at the same temperature the backward reaction is negligible), and not CO. This will lead to a high ortho-to-para H$_2$ conversion, consequently a lower ortho-to-para H$_2$ ratio as seen in Fig. 7. Our chemical modeling also predicts a variation of the steady-state ortho-to-para H$_2$ ratio for the complete depletion case, a depletion factor of 100 and a depletion factor of 10, between 9 and 16 K (see Fig. 7). Because of the large internal energy (~170 K) of the lowest ortho-H$_2$ level ($J = 1$) compared to the temperature range explored in this source, the ortho-H$_2$ form is a limiting factor for deuteration. It overcomes the energy barrier, leading to exothermic (i.e fast and temperature independent) reactions (e.g. Gerlich et al. 2002):
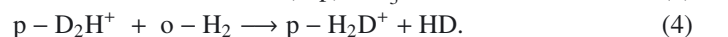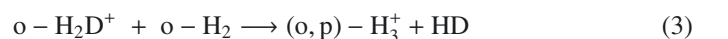
$$\mathrm{o-H_2D^+ + o-H_2 \longrightarrow (o,p)-H_3^+ + HD} \qquad (3)$$
$$\mathrm{p-D_2H^+ + o-H_2 \longrightarrow p-H_2D^+ + HD.} \qquad (4)$$

Table 2. Non-LTE computations for the ortho-H_2D^+, para- and ortho-D_2H^+ column densities for densities of 10^5, 5×10^5 and 10^6 cm^{-3}.

n_{H_2} (cm^{-3})	10^5	5×10^5	1×10^6
T_{gas} (K)	[12.7–15.6]	[9.9–12.2]	[9.4–11.2]
N(ortho-H_2D^+)	[1.4–1.9] $\times 10^{13}$	[1.2–1.8] $\times 10^{13}$	[1.2–1.9] $\times 10^{13}$
N(para-D_2H^+)	[1.7–2.9] $\times 10^{13}$	[1.1–2.4] $\times 10^{13}$	[1.1–2.3] $\times 10^{13}$
N(ortho-D_2H^+)	$\leq 1.6 \times 10^{14}$	$\leq 9.2 \times 10^{14}$	$\leq 5.1 \times 10^{14}$
[ortho-D_2H^+]/[para-D_2H^+]	≤ 6	≤ 44	≤ 32

Notes. The temperature range results from the intersection of the modeling (thin lines in Fig. 4) and the non-LTE computation (thick lines in Fig. 4).

The excited nuclear spin state of the D_3^+ ion is removed preferentially by ortho-H_2 in the following endothermic (by only 18 K) reaction:

$$m - D_3^+ + o - H_2 \longrightarrow o - D_2H^+ + HD. \qquad (5)$$
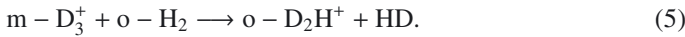
Following Hugo et al. (2009) we have assigned meta-D_3^+ with the modification having the lowest ground state energy, corresponding to the A1 representation of the symmetry group S3. All forms should be taken into account in any chemical modeling involving deuterated ions.

Although Pagani et al. (2009) showed that the ratio is unlikely in steady-state in prestellar cores, this will not affect the computation of the column densities since, as mentioned in Sect. 2, the collisional rates for ortho-H_2D^+ (as well as para- and ortho-H_2D^+) are similar for collisions with both para- and ortho-H_2. Note also that the difference between our modeling and Pagani et al. (2009) comes from the time-scale used. Our values are at equilibrium.

With a comparison between the chemical model predictions and the observations, three convergences can be found for the complete depletion case and $f_d = 100$. These domains are quoted in Table 2 for densities of 10^5, 5×10^5 and 1×10^6 cm^{-3}. From the gas kinetic temperature range (9.5–12.4 K) found from the uncertainties on the para-D_2H^+ and ortho-H_2D^+ linewidths, the $n_{H_2} = 10^5$ cm^{-3} domain can be ruled out. Should we consider the highest gas kinetic temperature (12.4 K) the modeling results in a para-D_2H^+/ortho-H_2D^+ abundance ratio 12% lower than the observations for a molecular density of 10^5 cm^{-3}. This would reduce the upper limit on the ortho-to-para ratio to a value of ~6, ~40% higher than the value modeled for the complete depletion case and with a depletion factor of 100 (see Fig. 5). Also, the comparison between the chemical modeling and the ortho-to-para D_2H^+ upper limit from the non detection of the ortho transition is consistent with a low gas temperature (<11.7 K for a 10^6 cm^{-3} density). A proper model should consider the (unknown) physical structure and proper time-depended freeze-out.

Note that no other molecular tracers like DCO^+ and N_2D^+, observed by Lis et al. (2002) can be used as a comparison with the chemical modeling as it might prove difficult to disentangle their contribution from the more extended envelope to the central region.

Considering an average 11 K gas temperature, the upper limit for the ortho-to-para D_2H^+ ratio is 2 to 3 times larger than the value found from the modeling (around 3) for densities larger than 10^5 cm^{-3}. We get, from the non-LTE radiative transfer modeling, N(ortho-H_2D^+) = $(1.4 \pm 0.1) \times 10^{13}$ cm^{-2}, N(para-D_2H^+) = $(1.4 \pm 0.2) \times 10^{13}$ cm^{-2}, and N(ortho-D_2H^+) $\leq 1.4 \times 10^{14}$ cm^{-2}. These values are reproduced by (or in the case of ortho-D_2H^+ compatible with) our chemical modeling in the complete depletion case. The present state of the art instruments are clearly unable to detect the ortho-D_2H^+ transition in

this source. The CCAT (Cornell Caltech Atacama Telescope[3]) project appears to be the most adequate to detect this ortho-D_2H^+ transition in warmer regions.

From Fig. 6, we can use the average 11 K gas temperature in the complete depletion case as well as with a depletion factor of 100 to estimate the radiation temperature of the para-H_2D^+ transition at 1370.085 GHz for densities larger than 10^5 cm^{-3}. Using a non LTE modeling described in Sect. 3.2, the resulting para-H_2D^+ column density is $(9.07 \pm 0.49) \times 10^{13}$ cm^{-2} ($T_R = (60\pm20)$ mK) for the complete depletion case, and $(3.40\pm0.19)\times 10^{13}$ cm^{-2} ($T_R = (50\pm10)$ mK) for a depletion factor of 100. This transition unfortunately falls in a frequency range not covered by the HIFI instrument, but could be a target for future instruments.

Carbon monoxyde in the LDN 1689N cloud is only moderately depleted in the single-dish beam (Lis et al. 2002) but it is possible that the angular resolution of the existing single-dish data is simply insufficient to show the spatial stratification predicted by our chemical model. The presence of completely depleted regions smaller than the CSO beam cannot be ruled out by our observations.

The deuterium peak in the LDN 1689N cloud has been argued in the literature to be a shock-compressed interaction region between a molecular outflow and an ambient cloud. Therefore high spatial resolution mapping observations of high density tracers, like NH_3 and its deuterated counterparts as well as N_2H^+ and N_2D^+ are necessary to allow investigating the kinematics of the high-density gas in this region. Both the Atacama Large Array Millimeter and Expanded Very Large Array are suitable for a follow-up of this source that reveals to be a non typical prestellar core.

4. Conclusions

1. The ground-state ortho-D_2H^+ $1_{1,1}$–$0_{0,0}$ transition at 1476.6 GHz in the prestellar core 16293E has been searched for with the *Herschel*/HIFI instrument.
2. The collision rates for the ortho and para H_2D^+ and D_2H^+ ions with molecular hydrogen have been used with a non-LTE radiative transfer code (RADEX) to derive the column densities of the detected ortho-H_2D^+ and para-D_2H^+ ground transitions as well as the upper limit on the ortho-D_2H^+ observed with the HIFI instrument on board the *Herschel* observatory.
3. We used a gas-phase chemical model, in which deuterium chemistry and the spin states have been added and compared our modeling with the inferred para-D_2H^+/ortho-H_2D^+, as well as the upper limit on the ortho-to-para D_2H^+ ratio. The kinetic temperature is deduced from the line width of both detected ions to be about 10 K, and we varied the molecular

[3] http://www.ccatobservatory.org/

hydrogen density between 10^5 and 10^6 cm^3. The upper limit on the observed ortho-to-para D_2H^+ ratio is consistent with the modeling and points to a low ($\sim$11 K) gas kinetic temperature. The detection of the ortho-D_2H^+ transition in the cold regime is a challenge as an rms of about 9 mK is needed, compared to the 21 mK rms reached by the HIFI instrument in about 5 h.

References

Amano, T., & Hirao, T. 2005, J. Mol. Spectr., 233, 7
Asvany, O., Ricken, O., Müller, H. S. P., et al. 2008, Phys. Rev. Lett., 100, 233004
Caselli, P., & Dore, L. 2005, A&A, 433, 1145
Caselli, P., van der Tak, F. F. S., Ceccarelli, C., & Bacmann, A. 2003, A&A, 403, L37
Caselli, P., Vastel, C., Ceccarelli, C., et al. 2008, A&A, 492, 703
Castets, A., Ceccarelli, C., Loinard, L., Caux, E., & Lefloch, B. 2001, A&A, 375, 40
Ceccarelli, C., & Dominik, C. 2005, A&A, 440, 583
Ceccarelli, C., Castets, A., Loinard, L., Caux, E., & Tielens, A. G. G. M. 1998, A&A, 338, L43
Ceccarelli, C., Vastel, C., Tielens, A. G. G. M., et al. 2002, A&A, 381, L17
Ceccarelli, C., Bacmann, A., Boogert, A., et al. 2010, A&A, 521, L22
de Graauw, T., Helmich, F. P., Phillips, T. G., et al. 2010, A&A, 518, L6
Draine, B. T., & Sutin, B. 1987, ApJ, 320, 803
Flower, D. R., Pineau des Forêts, G., & Walmsley, C. M. 2004, A&A, 427, 887
Flower, D. R., Pineau Des Forêts, G., & Walmsley, C. M. 2006, A&A, 449, 621
Fukui, Y., Sugitani, K., Takaba, H., et al. 1986, ApJ, 311, L85
Gérin, M., Pearson, J. C., Roueff, E., Falgarone, E., & Phillips, T. G. 2001, ApJ, 551, L193
Gerlich, D., Herbst, E., & Roueff, E. 2002, Planet. Space Sci., 50, 1275
Hirota, T., Ikeda, M., & Yamamoto, S. 2001, ApJ, 547, 814
Hugo, E., Asvany, O., & Schlemmer, S. 2009, J. Chem. Phys., 130, 164302
Lis, D. C., Gerin, M., Phillips, T. G., & Motte, F. 2002, ApJ, 569, 322
Lis, D. C., Gerin, M., Roueff, E., Vastel, C., & Phillips, T. G. 2006, ApJ, 636, 916
Loinard, L., Castets, A., Ceccarelli, C., Caux, E., & Tielens, A. G. G. M. 2001, ApJ, 552, L163
Loinard, L., Torres, R. M., Mioduszewski, A. J., & Rodríguez, L. F. 2008, ApJ, 675, L29
Loren, R. B., Wootten, A., & Wilking, B. A. 1990, ApJ, 365, 269
Menten, K. M., Serabyn, E., Guesten, R., & Wilson, T. L. 1987, A&A, 177, L57
Mizuno, A., Fukui, Y., Iwata, T., Nozawa, S., & Takano, T. 1990, ApJ, 356, 184
Ott, S. 2010, in Astronomical Data Analysis Software and Systems XIX, eds. Y. Mizumoto, K.-I. Morita, & M. Ohishi, ASP Conf. Ser., 434, 139
Pagani, L., Vastel, C., Hugo, E., et al. 2009, A&A, 494, 623
Parise, B., Ceccarelli, C., Tielens, A. G. G. M., et al. 2002, A&A, 393, L49
Parise, B., Castets, A., Herbst, E., et al. 2004, A&A, 416, 159
Phillips, T. G., & Vastel, C. 2003, in SFChem 2002: Chemistry as a Diagnostic of Star Formation, eds. C. L. Curry, & M. Fich, 3
Pilbratt, G. L., Riedinger, J. R., Passvogel, T., et al. 2010, A&A, 518, L1
Ramanlal, J., & Tennyson, J. 2004, MNRAS, 354, 161
Roberts, H., & Millar, T. J. 2000, A&A, 361, 388
Roberts, H., Herbst, E., & Millar, T. J. 2003, ApJ, 591, L41
Roberts, H., Herbst, E., & Millar, T. J. 2004, A&A, 424, 905
Roelfsema, P. R., Helmich, F. P., Teyssier, D., et al. 2012, A&A, 537, A17
Roueff, E., Tiné, S., Coudert, L. H., et al. 2000, A&A, 354, L63
Roueff, E., Lis, D. C., van der Tak, F. F. S., Gerin, M., & Goldsmith, P. F. 2005, A&A, 438, 585
Saito, S., Ozeki, H., Ohishi, M., & Yamamoto, S. 2000, ApJ, 535, 227
Sipilä, O., Hugo, E., Harju, J., et al. 2010, A&A, 509, A98
Stark, R., Sandell, G., Beck, S. C., et al. 2004, ApJ, 608, 341
Taquet, V., Ceccarelli, C., & Kahane, C. 2012, ApJ, 748, L3
Tielens, A. G. G. M. 1983, A&A, 119, 177
Turner, B. E. 1990, ApJ, 362, L29
van der Tak, F. F. S., Schilke, P., Müller, H. S. P., et al. 2002, A&A, 388, L53
van der Tak, F. F. S., Black, J. H., Schöier, F. L., Jansen, D. J., & van Dishoeck, E. F. 2007, A&A, 468, 627
Vastel, C., Phillips, T. G., Ceccarelli, C., & Pearson, J. 2003, ApJ, 593, L97
Vastel, C., Phillips, T. G., & Yoshida, H. 2004, ApJ, 606, L127
Wakelam, V., Herbst, E., Loison, J.-C., et al. 2012, ApJS, 199, 21
Walmsley, C. M., Flower, D. R., & Pineau des Forêts, G. 2004, A&A, 418, 1035
Wootten, A., & Loren, R. B. 1987, ApJ, 317, 220